International Journal of Information Acquisition
Vol. 2, No. 3 (2005) 191–201
© World Scientific Publishing Company

World Scientific
www.worldscientific.com

# DESIGN, MODELING AND IMPLEMENTATION OF PbPc SENSOR ARRAY FOR THE DETECTION OF GASES

MAHMOUD Z. ISKANDARANI
*Faculty of Science and Information Technology*
*Al-Zaytoonah Private University of Jordan*
*P.O. Box 911597, Post Code 11191, Jordan*
*m_iskandarani@yahoo.com*

NIDAL F. SHILBAYEH
*Faculty of Information Technology for Graduate Studies*
*Jordan University for Graduate Studies*
*P.O. Box 41, Post Code 11931, Amman, Jordan*
*n_shilbayeh@yahoo.com*

Received 7 May 2005
Accepted 1 September 2005

In this paper the voltage/current characteristics and the effect of $NO_2$ gas on the electrical conductivity of a PbPc gas sensor array is studied. The gas sensor is manufactured using vacuum deposition of gold electrodes on sapphire substrate with the lead-phathalocyanine vacuum sublimed on the top of the gold electrodes. In a comparison between two versions of the PbPc gas sensor array, it was found that they differ in gap sizes between the deposited gold electrodes. The sensors are tested at different temperatures to account for conductivity changes as the molecular adsorption/desorption rate is affected by heat. The obtained results are found to be encouraging as the sensors showed stability and sensitivity towards low concentrations of applied $NO_2$ gas.

*Keywords*: Intelligent system; PbPc; gas sensor; mathematical modeling.

## 1. Introduction

The gases absorbed on the surfaces of the organic materials have a marked effect on the electrical conductivity of these materials, where the electrical conductivity of an organic material that contains transition and heavy central atoms changes by many orders of magnitude when a gas adsorbs on its surface.

Adsorption involves the formation of bonds between the adsorbed gas and the organic material by the transfer of electrical charge. The charge transfer changes the electronic structure of the material, thus changing its conductivity. Changes in the conductivity are related to the number of gas molecules adsorbed on the surface, and hence, to the concentration of the

adsorbed species in the surrounding atmosphere. The measurement of changes in electrical conductance due to gas adsorption makes organic materials ideal for the detection of low gas concentration.

The conductivity of an organic material can either be affected at the surface with no bulk interaction, or following the reaction at the surface; carriers can be injected into the bulk causing both surface and bulk conductivities to be affected [Carotta *et al.*, 2001; Hatfield *et al.*, 2000; Gardner *et al.*, 1999].

When a gas molecule chemisorbs on the surface of the organic material, an electron or several electrons may be transferred from one to the other, where the direction of transfer depends on the electronegativity of the gas and the work function of the solid. Also the physisorption of the gas plays an important role in the overall mechanism of gas adsorption and subsequent conductivity changes in the organic material. The adsorption of the gas molecules as ions on the surface removes electrons from the solid and localizes them at the surface, thus generating electron traps in the solid. This results in an increase in the hole concentration and therefore an increase in the conductance as the material will function as a P-type material [Mirtaheri *et al.*, 2004, Marian *et al.*, 2001].

In this paper the properties of the PbPc sensor array is confirmed, modeled, and employed in an intelligent discriminating and controlling system. The system uses the inter-digital geometry together with PbPc film properties to distinguish between types of gases.

## 2. Background

### 2.1. *Metal-phthalocyanines*

Metal-phthalocyanines are a group of organic materials known to have several properties that make them attractive as a potential gas sensing materials or gas detectors. They have the following desirable properties:

- They are considered to be good electrical conductors, where the charge carriers are known to be positive holes [Gutierrez-Osuna & Powar, 2003; Gutierrez-Osuna & Gutierrez-Galvez, 2003; Gardner & Iskandarani, 1992].
- Reaction of phthalocyanines with electron accepting gases should increase its conductivity.
- They are thermally stable to temperatures in excess of 400°C.
- They can be used for extended periods at elevated temperatures.
- Organic groups can be easily modified and functional groups can be substituted on either ring structure or on the central hydrogen atom in the metal-free phthalocyanines ($H_2Pc$).

Several of the metal-phthalocyanine materials (e.g. commercial materials) contain significant amounts of impurities which can result in irreproducible electrical characteristics, which can be purified using either gas-entrainer sublimation (in nitrogen or oxygen) or by vacuum sublimation (the used technique in our work). The purification process leads to stable and reproducible electrical characteristics. Early studies of phthalocyanines showed that many are sensitive to the presence of $NO_2$with an increase in the sensitivity observed when the phthalocyanines contains heavier central atoms.

Metal-phthalocyanines organic semiconductors are found to undergo conductivity changes upon the adsorption of strongly electrophilic gases such as $NO_2$, $Cl_2$ and $F_2$. The magnitude and reversibility of these conductivity variations are found to be dependant on the central metal species. Because of their high decomposition temperatures (450°C), phthalocyanines can be vacuum evaporated to produce thin films. The deposition of such films on the surface of a substrate eliminates some of the complications arising from having to consider both surface and bulk conductivities in the analysis process. The absence of bulk conductivity effect will improve the response and recovery times of the designed sensor array. However, the presence of impurities will affect resistivity, linearity, hysterisis and drift of the electrical characteristics. In addition the conduction activation energy and the specific conduction mechanism will be affected.

Changes in conductivity are caused by electron transfer between adsorbed molecules and

the semiconductor surface. The electrical conduction takes place via individual $SnO_2$ grains. $NO_2$ gets chemisorbed at the surface of $SnO_2$ grains. Hereby they trap electrons at the surface. $SnO_2$ in an n-type semiconductor. Hence the trapping of the free electrons causes a decrease in free charge carrier concentration and therefore an increase in the sensor resistance.

### 2.2. *Lead-phthalocyanines (PbPc)*

Lead-phthalocyanines are the most sensitive and stable Phthalocyanine materials. Although, insensitive to a wide range of gases (e.g. weak electrophilic and electrophobic gases and $CH_4$, CO, $CO_2$, $H_2O$, $H_2$, hydrocarbons and changes in $O_2$ pressure), the PbPc based sensor is very sensitive and is potentially useful in detecting strong electrophilic gases particularly to $NO_2$ or $NO_x$ and will respond to low concentrations of $F_2$ and less than 1 ppm concentration of $Cl_2$ gases. Thus it could form the basis of a highly sensitive and selective $NO_2$ or $NO_x$ sensor and it is suitable for detecting these gases at concentrations from 1 ppb to 10 ppm in air and retains discrimination to concentrations above 100 ppm.

Since PbPc has high sensitivity and selectivity to strongly accepting gases such as $NO_2$, $Cl_2$, $F_2$ and $O_3$, discrimination between strongly accepting gases and other gases is achieved by careful choice of operating temperatures. However, the stability and electrical properties of this type of sensors is affected by water vapor, so a heating element is usually fitted to the back of the sensor to eliminate such a factor.

It is found [Gardner & Iskandarani, 1992] that PbPc sensor is most sensitive to $NO_2$ gas and can be operated in a continuous mode at temperatures above 100°C with its sensitivity and stability decreasing as the temperature approaches 200°C. These temperatures are also a function of PbPc film thickness deposited on the substrate and can be extended when thick films are used.

## 3. PbPc Sensor Design

The sensor is based on a sapphire substrate (Alpha-$Al_2O_3$), which usually contains traces of Fe and Ti ions. The substrate has a very high melting point (about 2050°C). It is very hard and quite inert, especially towards acids. The substrate has an area of 12.5 mm by 12.5 mm. Different types of electrode gap separations are produced to study the effect of inter-electrode separation of sensor sensitivity as shown in the SEM photographs in Figs. 1, 2 and 8(a).

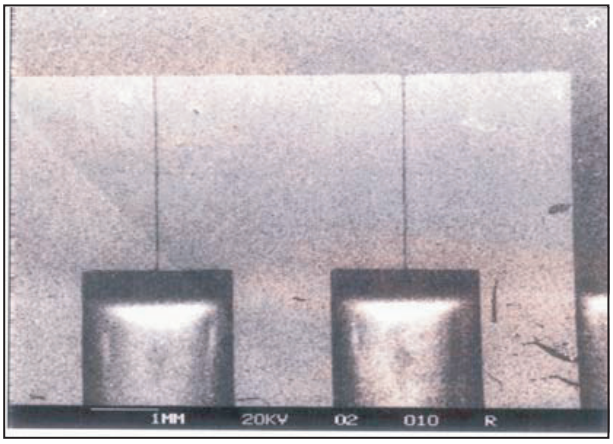


Fig. 1. 10:10:10 gap ratio.

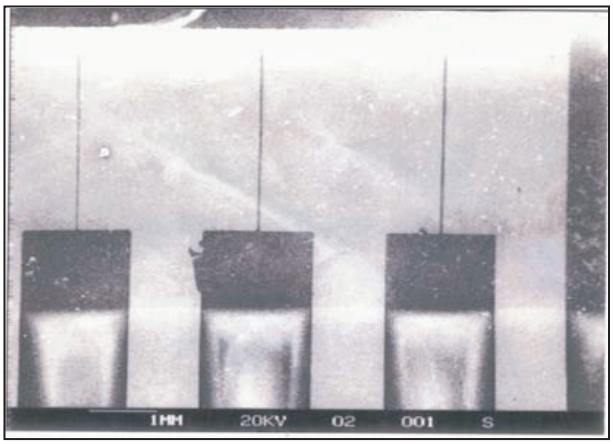


Fig. 2. 5:10:15 gap ratio.

Masks were made from a material called STABILENE to produce the following parts forming the overall device:

(a) Contact pads
(b) Device structure (finite co-planar electrode configuration)
(c) Pads and PbPc windows

To enable the above patterns to be transferred to the substrate surface, the masks have

to be reduced first in size and their images printed on glass slides over two stages:

(i) First stage reduction is carried out using the "first reduction camera". Each mask is placed in turn on a screen with a high resolution Kodak type (1A) glass plate held by a vacuum supplied through a pipe. To obtain a clear image, the camera focus and the distance between lenses and mask are adjusted and set to appropriate values. Light is then passed through the mask for duration of time controlled by a timing device, then projected through the lenses onto the glass plate. The exposing time was chosen carefully so the image was not under or overexposed.
(ii) A second stage reduction is also carried out using a "second reduction camera" (step and repeat camera), where a process of multiplication is employed.

Metal deposition using electron beam evaporation is a conventional method of depositing metal films. The process is carried out under vacuum in an Edwards evaporator. The evaporating apparatus consists simply of a circular filament and a crucible for the material to be evaporated. The crucible is held at earth potential and the filament at a high negative potential that accelerates electrons from the filament to strike the material in the crucible. The impact of these electrons heat the material to its melting point, and evaporation then occurs, the material sublimes into a thin film covering the required surface area of the wafer (using the e-beam method and under $5 \times 10^{-6}$ Torr vacuum).

After metal deposition, the wafer was coated with positive photoresist (Shipley Tf-16). The device is then spun. The spinner used consists of a small electrical motor driven from the mains with a speed controller. A vacuum pump is used to hold the substrate to the rotating part of the spinner for one or several small substrates, while a larger revolving part with a push fit restrainer was used with larger size and/or larger number of substrates.

After photoresist deposition the wafer was soft baked. This process generally known as pre-baking is used to improve adhesion and remove solvent from the photoresist. After prebaking, the photoresist is ready for mask alignment and exposure. So the wafer is placed in the mask aligner which has the function of transferring the mask pattern to the photoresist coated wafer, with the pads mask laid above the wafer and aligned visually using the optical arrangement. When aligned, the substrate is held in place by vacuum. The mask and substrate are then exposed to ultraviolet. The exposed wafer is then developed in Shipley Mf-319 (undiluted) solution. Thereafter the wafer is hard baked in order to harden the photoresist and further improve adhesion to the substrate. The same wafer is put in the evaporator under high vacuum and Au is deposited.

The wafer is coated again with Tf-16 positive photoresist, spun at high speed, and then soft baked. Thereafter the wafer and the device mask are placed in the mask aligner, exposed to ultraviolet light, developed in Shipley Mf-319 and then hard baked. The wafer is then etched to produce the device gold structure. The extra photoresist is removed using acetone.

S1813, a negative photoresist is applied to the wafer which is then spun at high speed and then soft baked. Thereafter, the wafer and the windows mask are placed in the mask aligner, exposed to ultraviolet light, then developed in Shipley 351. The wafer is then hard baked. Resist at this stage is not removed from the device; only pads and PbPc windows are cleared of resist.

## 4. Experimental Setup

The sensor is mounted on a transistor like base as shown in Fig. 3, as it comprises of three gaps. A testing chamber is built with air and temperature controls supplied through a computer controlled unit.

Electrical characteristics of the sensor and its response to gases are recorded via specially designed hardware/software system as shown in Fig. 4 [Cole *et al.*, 1999; Hines *et al.*, 1999; Dyer & Gardner, 1997; Gardner *et al.*, 1996].

The DC conductivity sensor consists of a resistive layer, which is deposited on top of

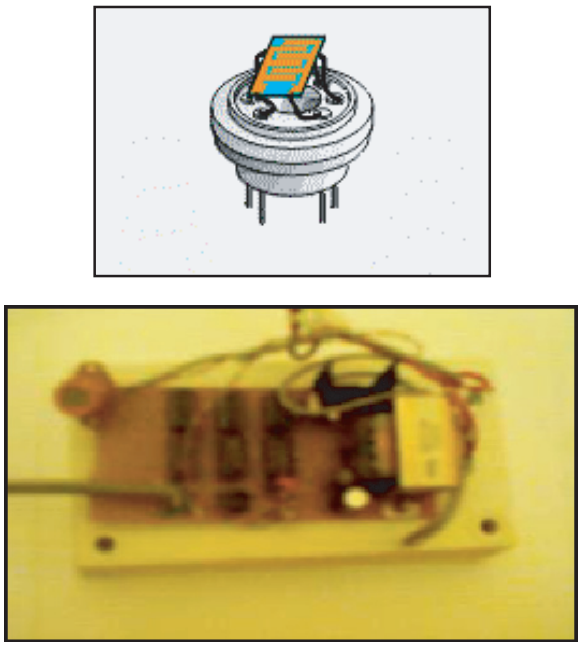

Fig. 3. Sensor mounting.

the electrode structure. The substrates can be miniaturized and mounted on commercial standard sockets.

Gases in the atmosphere interact with the resistive layer. The gases get absorbed onto the sensor surface and, depending on the nature of their interaction electrons are trapped or released into the bulk. Changes in the ambient atmosphere reflect the changes in the sensor resistance. The gas-sensor interaction is shown in Fig. 5.

The measured conductivity is a combination of a conductivity contribution of the surface, which is affected by the gas, and a conductivity contribution of the bulk, which is typically

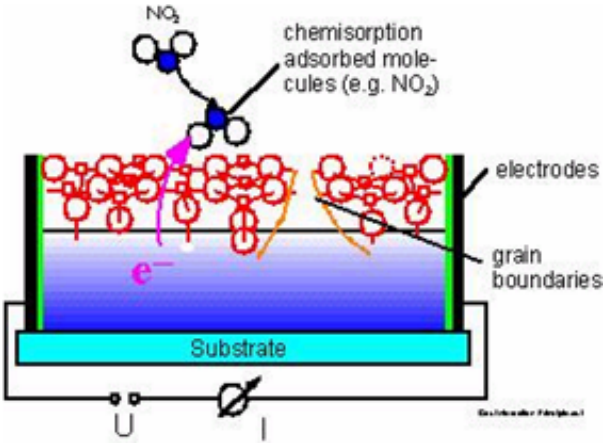


Fig. 5. Sensor interaction with $NO_2$ gas.

unaffected at the operation temperature of the sensor.

### 4.1. *Sensor interface circuit*

The obtained signals from the PbPc sensor array is known to have relatively small values, hence, a differential amplifier interface circuit is designed and used to condition the sensor output signal to the remaining part of the signal processing system, which also includes A/D converter and noise filters. The basic amplifying unit is shown in Fig. 6 [Perera *et al.*, 2002; Gardner *et al.*, 2000; Gutierrez-Osuna & Nagle, 1999].

In Fig. 6 two inter electrodes each produces a voltage signal proportional to the gap size and film thickness of the deposited PbPc film. The difference in the voltage of each electrode is amplified and processed to the next stage. The amplifying unit acts as an impedance matcher,

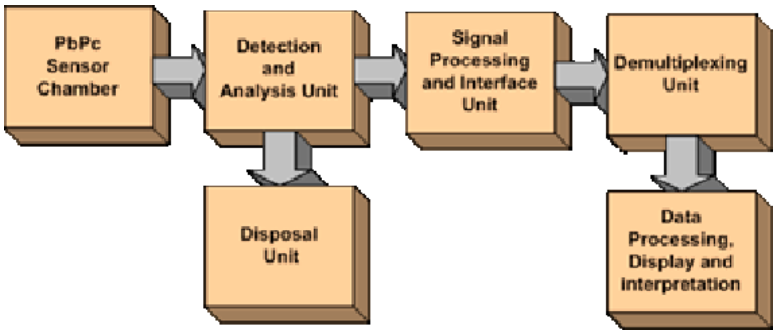


Fig. 4. Testing system.

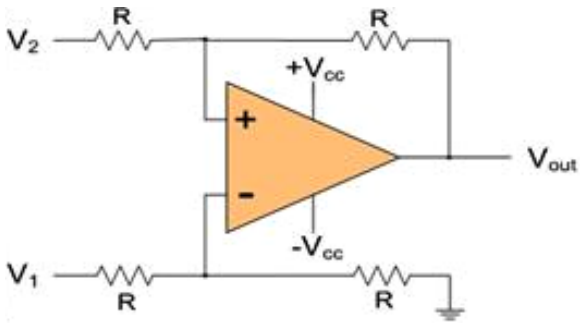


Fig. 6. Differential amplifier interface unit.

so that a correct measure of the detected gas level is acquired with minimal signal loss.

### 4.2. *Interfacing algorithm*

After digitizing the amplified and cleaned sensor array signals, they are processed to be analyzed using the algorithm shown in Fig. 7.

## 5. Mathematical Modeling

To model the behavior of our multi-gap sensor, a form of linear transformation is used to transform a unit circle of the Z-plane to the upper half ($I_m > 0$) of the W-plane as shown in Figs. 8(a) and 8(b).

Consider the transformation:

$$z = x + jy = f(t) = j \cdot \left(\frac{1-t}{1+t}\right), \qquad (1)$$

thus

$$t = -\left(\frac{z-j}{z+j}\right). \qquad (2)$$

Now, if $(x_1)$ is any general point on the X-axis of the Z-plane and if it is represented in its polar form with a corresponding angle of $(\theta_1)$ then, Eq. (2) can be written as:

$$e^{j\theta_1} = -\left(\frac{x_1 - j}{x_1 + j}\right) \qquad (3)$$

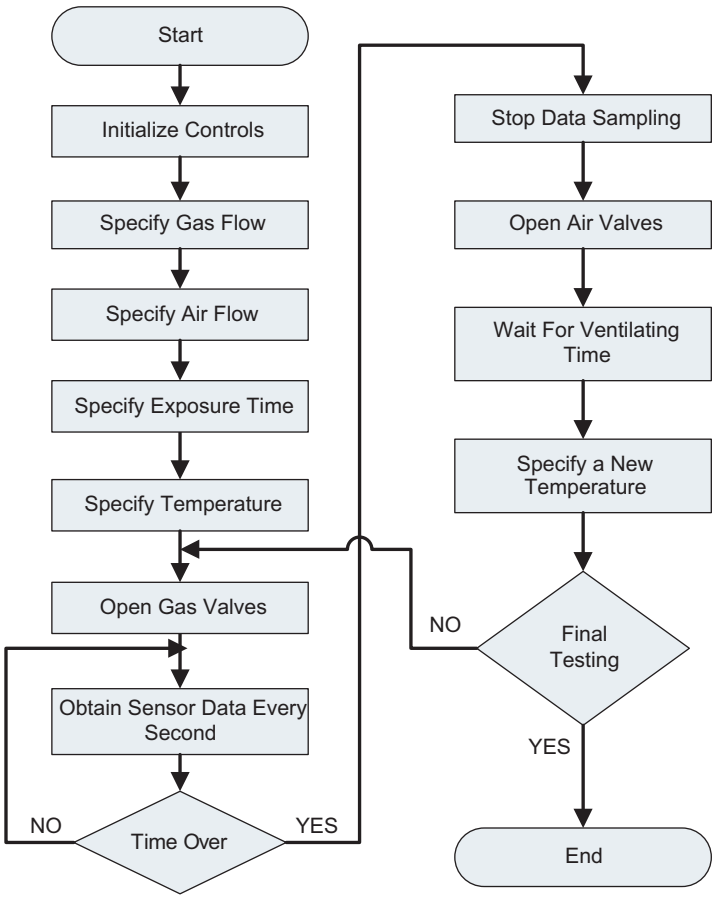


Fig. 7. Interface algorithm.

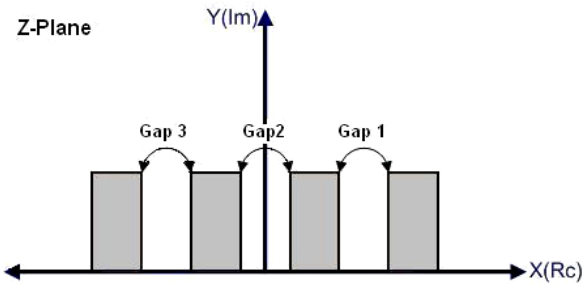


Fig. 8(a). Inter-electrode gap separations.

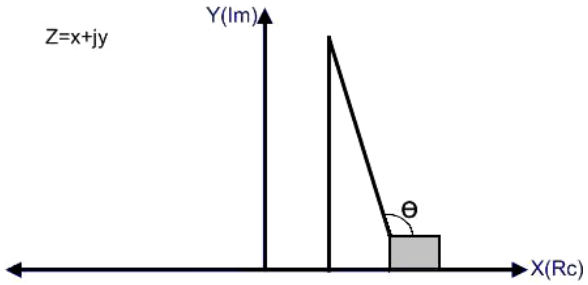


Fig. 8(b). Inter-electrode angle.

and thus,

$$\theta_1 = j \ln\left(\frac{x_1 - j}{x_1 + j}\right). \tag{4}$$

Whence,

$$\begin{aligned} d\theta_1 &= j\left(\frac{x_1 + j}{x_1 - j}\right)\left(\frac{-2dx_1}{(x_1 + j)^2}\right) \\ &= \left(\frac{2dx_1}{(1 + x_1^2)}\right). \end{aligned} \tag{5}$$

Now, the SCHWARZ complex potential solution $W = \theta + j\psi$ is obtained through the following evaluation:

$$W = \frac{1}{2\pi}\int_{-\infty}^{+\infty}\left(\frac{e^{j\theta_1} + t}{e^{j\theta_1} - t}\right)\varphi(x_1)\, d\theta_1. \tag{6}$$

Substituting Eqs. (2), (3) and (4) into (6) gives:

$$W = \frac{1}{2\pi}\int_{-\infty}^{+\infty}\left(\frac{-(1 + x_1 z)}{j\,(z - x_1)}\right)\left(\frac{2dx_1}{(1 + x_1^2)}\right)\varphi(x_1), \tag{7}$$

$$W = \frac{j}{\pi}\int_{-\infty}^{+\infty}\left(\frac{(1 + x_1 z)}{(1 + x_1^2)(z - x_1)}\right)\varphi(x_1)\, dx_1. \tag{8}$$

This is a solution of the first boundary value problem of the first kind in the upper half of the W-plane. The real part in Eq. (8) is:

$$\varphi(x, y) = \frac{1}{\pi}\int_{-\infty}^{+\infty}\left(\frac{y}{(x - x_1)^2 + y^2}\right)\varphi(x_1)\, dx_1. \tag{9}$$

Equation (9) represents a Poisson's integral formula for the upper half-plane, and for an array of $(i + 1)$ electrodes separated by gaps $g_1, g_2, \ldots, g_i$, Eq. (9) becomes

$$\begin{aligned} \varphi(x, y) = \Bigg[\varphi_0 \frac{y}{\pi}\int_{-\infty}^{+\infty}&\left(\frac{dx_1}{(x - x_1^2) + y^2}\right) \\ &\times \varphi_1 \frac{y}{\pi}\int_{g_1}^{g_2}\left(\frac{dx_2}{(x - x_2^2) + y^2}\right) + \cdots \\ &+ \varphi_i \frac{y}{\pi}\int_{g_i}^{+\infty}\left(\frac{dx_i}{(x - x_i^2) + y^2}\right)\Bigg]. \end{aligned} \tag{10}$$

Equation (10) can be solved to give:

$$\begin{aligned} &\left(\frac{\varphi_0 + \varphi_1}{2}\right) + \left(\frac{\varphi_0 - \varphi_1}{\pi}\right)\tan^{-1}\left(\frac{g_1 - x}{y}\right) \\ &\quad + \left(\frac{\varphi_1 - \varphi_2}{\pi}\right)\tan^{-1}\left(\frac{g_2 - x}{y}\right) + \cdots \\ &\quad + \left(\frac{\varphi_{i-1} - \varphi_i}{\pi}\right)\tan^{-1}\left(\frac{g_i - x}{y}\right). \end{aligned} \tag{11}$$

To find the complex solution $W = \theta + j\psi$ and the field expression, Eq. (11) is rearranged and written taking into account the following gaps arrangement:

$$\tan^{-1}\left(\frac{g_l - x}{y}\right) = \varphi_l = (\varphi_l - \pi/2), \tag{12}$$

where $\theta_l = \arg(z - g_l)$ is the angle between $(z - g_l)$ and the positive X-axis. Then,

$$\begin{aligned} \varphi(x, y) &= \varphi_i + \left(\frac{\varphi_0 - \varphi_1}{\pi}\right)\theta_1 + \cdots + \left(\frac{\varphi_{i-1} - \varphi_i}{\pi}\right)\theta_i \\ &= \sum_{n=1}^{i}\varphi_i + \left(\frac{\varphi_{n-1} - \varphi_n}{\pi}\right)\theta_n, \end{aligned} \tag{13}$$

and

$$\begin{aligned}\varphi(x,y) &= \varphi_i + \left(\frac{\varphi_0-\varphi_1}{\pi}\right)\arg(z-g_1)+\cdots \\ &\quad + \left(\frac{\varphi_{i-1}-\varphi_i}{\pi}\right)\arg(z-g_i) \\ &= \sum_{n=1}^{i}\varphi_i + \left(\frac{\varphi_{n-1}-\varphi_n}{\pi}\right)\arg(z-g_n).\end{aligned} \tag{14}$$

Now, Eq. (14) has the following equivalent electrical transformation:

$$\begin{aligned}&[\varphi(x,y)-\varphi_i] \\ &\quad = \mathrm{Re}\left[\frac{-j}{\pi}\sum_{n=1}^{i}(\varphi_{n-1}-\varphi_n)\ln(R_n)+j\theta_n\right].\end{aligned} \tag{15}$$

When $R$ and $\theta$, are polar coordinates and

$$\begin{aligned}R_l &= \left[\left(x^2-g_l^2\right)+y^2\right]^{1/2} \\ \theta_l &= \tan^{-1}\left[\frac{g_l-x}{y}\right],\end{aligned} \tag{16}$$

substituting Eqs. (16) into (15) yields:

$$\varphi(x,y) = \sum_{n=1}^{i}\varphi_i + \left(\frac{\varphi_{n-1}-\varphi_n}{\pi}\right)\theta_n. \tag{17}$$

Now from Eqs. (15), (16) and (17) we can deduce the complex potential as:

$$\begin{aligned}W &= \varphi + j\psi \\ &= \sum_{n=1}^{i}\varphi_i + \left(\frac{\varphi_{n-1}-\varphi_n}{\pi}\right)\ln(z-g_n),\end{aligned} \tag{18}$$

and,

$$\begin{aligned}|\underline{\mathrm{E}}| &= \left|-j\overline{\frac{dw}{dz}}\right| = \sum_{n=1}^{i}\left(\frac{\varphi_{n-1}-\varphi_n}{\pi}\right)\left(\overline{\frac{1}{z-g_n}}\right) \\ &= \left|-j\sum_{n=1}^{i}\left(\frac{\varphi_{n-1}-\varphi_n}{\pi}\right)\left(\frac{(x-g_n)+jy}{(x-g_n)^2+y^2}\right)\right|.\end{aligned} \tag{19}$$

Then,

$$|\underline{\mathrm{E}}| = \left|-j\sum_{n=1}^{i}\left(\frac{\varphi_{n-1}-\varphi_n}{\pi}\right)\left(\frac{z-g_n}{|z-g_n|^2}\right)\right|. \tag{20}$$

Equation (20) is solved to give:

$$\begin{aligned}|\underline{\mathrm{E}}| &= \left[\sum_{n=1}^{i}\left[\left(\frac{\varphi_{n-1}-\varphi_n}{\pi}\right)\left(\frac{(x-g_n)}{(x-g_n)^2+y^2}\right)\right]\right. \\ &\quad \left. + \left[\left(\frac{\varphi_{n-1}-\varphi_n}{\pi}\right)\left(\frac{y}{(x-g_n)^2+y^2}\right)\right]\right]^{1/2}.\end{aligned} \tag{21}$$

From Eq. (21):

(I)

$$\begin{aligned}&x = g_n, \\ &|\underline{E}| = E_y = \left[\sum_{n=1}^{i}\left(\frac{\varphi_{n-1}-\varphi_n}{\pi}\right)^2\left(\frac{1}{y}\right)^2\right]^{1/2} \\ &\quad = \left[\sum_{n=1}^{i}\left(\frac{\varphi_{n-1}-\varphi_n}{\pi}\right)\left(\frac{1}{y}\right)\right].\end{aligned} \tag{22}$$

Here, the field is only dependent on the Y-axis with no gaps realized, it is a bisecting field which varies between $\infty$ and 0 as $y$ takes on values between 0 and $\infty$.

(II)

$$\begin{aligned}&y = 0, \\ &|\underline{E}| = E_x = \left[\sum_{n=1}^{i}\left(\frac{\varphi_{n-1}-\varphi_n}{\pi}\right)\left(\frac{1}{x-g_n}\right)\right].\end{aligned} \tag{23}$$

The field in this case has a pole at $(x = g_n)$ for which Eq. (23) is infinite.

(III)

$$\begin{aligned}&x \gg g_n, \\ &E_x = \left[\sum_{n=1}^{i}\left(\frac{\varphi_{n-1}-\varphi_n}{\pi}\right)\left(\frac{1}{x}\right)\right].\end{aligned} \tag{24}$$

Here the field has total dependency on $x$ and it is parallel:

(IV)

$$\begin{aligned} x &= 0, \\ |\underline{E}| &= E_y \\ &= \left[\sum_{n=1}^{i}\left(\frac{\varphi_{n-1}-\varphi_n}{\pi}\right)\left(\frac{1}{y^2+g_n^2}\right)^{1/2}\right]. \end{aligned} \tag{25}$$

Equation (25) describes the field bisecting the gaps and electrodes:

(V) $y \gg g_n$, Equation (25) is reduced to (22).

(VI)

$$\begin{aligned} x &= y = 0, \\ |\underline{E}| &= E_{origin} \\ &= \left[\sum_{n=1}^{i}\left(\frac{\varphi_{n-1}-\varphi_n}{\pi}\right)\left(\frac{1}{g_n}\right)\right]. \end{aligned} \tag{26}$$

Here the field is completely controlled by the gaps.

Now by integrating Eq. (26) and dividing by $\varphi_{n-1}-\varphi_n = \Delta v_n$, we obtain:

$$G' = \sum_{n=1}^{i}\left(\frac{i'_n}{\Delta v_n}\right) = \frac{\sigma}{\pi}\sum_{n=1}^{i}\ln\left[\left(\frac{y_k^2}{g_n^2}\right)^{1/2}+\frac{y_k}{g_n}\right], \tag{27}$$

when $y_k$ can be chosen to represent the film thickness.

Using the temperature dependent general equation

$$\sigma = \sigma_0 \exp\left(-\left[\frac{T_0}{T}\right]^{0.25}\right), \tag{28}$$

where $\sigma_0$, $T_0$ are functions of Fermi levels.

Now, substituting Eq. (28) into (27) gives

$$G' = \left[\frac{\sigma_0}{\pi}\exp\left(\frac{-T_0}{T}\right)^{0.25}\right] \times \sum_{n=1}^{i}\ln\left[\left(\frac{y_k^2}{g_n^2}+1\right)^{1/2}+\frac{y_k}{g_n}\right]. \tag{29}$$

We can also represent the effect of activation energy through Arrhenius behavior:

$$\sigma = A\exp\left(\frac{-E_a}{KT}\right), \tag{30}$$

where $E_a$ is the activation energy.

Equation (27) becomes:

$$G' = \left[\frac{A}{\pi}\exp\left(\frac{-E_a}{KT}\right)\right]\sum_{n=1}^{i}\ln\left[\left(\frac{y_k^2}{g_n^2}\right)^{1/2}+\frac{y_k}{g_n}\right]. \tag{31}$$

Equation (31) expresses conductivity in terms of temp, gap width, and film thickness.

## 6. Discussion and Conclusion

Table 1 show the testing results of our array sensor using $NO_2$ gas as the testing substance under normal atmospheric pressure and over temperatures ranging from 110°C up to 150°C.

Table 1. Sensor conductance/concentration.

| Gas concentration ppm | Sensor array conductance ohms$^{-1}$ at 110°C | | | Sensor array conductance ohms$^{-1}$ at 130°C | | | Sensor array conductance ohms$^{-1}$ at 150°C | | |
|---|---|---|---|---|---|---|---|---|---|
| | Gap 5 | Gap 10 | Gap 15 | Gap 5 | Gap 10 | Gap 15 | Gap 5 | Gap 10 | Gap 15 |
| 0 | 332.2 | 469.9 | 582.9 | 308.1 | 337.7 | 361.7 | 81.1 | 167.2 | 236.2 |
| 1 | 1071.2 | 1354.1 | 1853.2 | 1267.8 | 1445.1 | 1518.3 | 327.3 | 679.7 | 882.3 |
| 3 | 1733.1 | 2164.5 | 3355.7 | 2340.3 | 2785.5 | 2939.4 | 753.2 | 1620.5 | 1834.2 |
| 5 | 2411.4 | 2670.9 | 4480.3 | 3111.4 | 3601 | 3790.8 | 1406.3 | 2503.1 | 2523.9 |
| 7 | 3282.9 | 3614.1 | 5379.2 | 3522.4 | 4196.4 | 4490.4 | 1445.1 | 3099.8 | 3448.3 |
| 9 | 3457.8 | 4096.7 | 5779.1 | 3996.8 | 4486.3 | 4990 | 2480.2 | 3671.1 | 3906.3 |

It clearly indicates an increase in the output signal response of the sensor as a function of three main factors:

(i) Distance between conducting electrodes (inter-digital separation)
(ii) Increase in atmospheric temperature
(iii) Effect of gas concentration

These factors can be used to control the behavior of the sensor in terms of the amount and type of adsorbed odors and the rate of desorption. The table also shows that the increase in output signal current is exponential. The mathematical law governing the response of the sensor is affected by the way the Organic Semi conducting layer is sublimed as well as its thickness and uniformity.

Overall, the obtained characteristics of the tested groups of sensors very much agree with the literature and proves the response shape of such sensor to be a specific case of power law response, which is a real exponential. Each sensor can be modeled as a group of three sensors grouped together which initiates the need to use pattern recognition and smart classification techniques [Gutierrez-Osuna *et al.*, 2003; Cole *et al.*, 2001; Shin *et al.*, 2000].

A suggested neural model would associate the three previously mentioned important parameters, which would implicitly determine gas concentration level and its type. Such a model should allow the process of discrimination between different types of gases and would be able to establish the level of detected gas [Gardner *et al.*, 1998, 1999; Llobet *et al.*, 1999a, 1999b; Hines *et al.*, 1999a; Dyer & Gardner, 1997; Vlachos *et al.*, 1996].

## References


Boilot, E. L., Gardner, H. and Gardner, J. W. [2001] "Knowledge extraction from electronic nose data sets using hybrid neuro-fuzzy systems," in *Sensors Update*, 8, H. Baltes, W. Gpel, J. Hesse (Series Eds.), Wiley-VCH Verlag GmbH, Weinheim, pp. 73–94, ISBN 3-527-30258-1 (C).

Carotta, M. C., Martinelli, G., Crema, L., Malagù, C., Merli, M., Ghiotti, G. and Traversa, E. [2001] "Nanostructured thick film gas sensors for atmospheric pollutant monitoring: Quantitative analysis on field tests," *Sensors and Actuators B* **76**, 336–342.

Cole, M., Gardner, J. W., Lim, A. W. Y., Scivier, P. K. and Brignell, J. E. [1999] "Polymeric resistive bridge gas sensor array driven by a standard cell CMOS current drive chip," *Sensors and Actuators B* **58**, 518–525 (JR).

Cole, M., Gardner, J. W., Dyer, D. C. and Bartlett, P. N. [2001] "Low-drift odour and vapour ratiometric resistive elements for analogue CMOS smart sensors," *8th International Symposium on Olfaction and the Electronic Nose*, 25–30 March, Washington DC, USA.

Dyer, D. C. and Gardner, J. W. [1997] "High precision intelligent interface for a hybrid electronic nose," *Sensors and Actuators B* **62**, 724–728 (JR).

Gardner, J. W., Craven, M., Dow, C. and Hines, E. L. [1998] "The prediction of bacteria type and culture growth phase by an electronic nose with a multi-layer perceptron network," *Measurement Science and Technology* **9**, 120–127 (JR).

Gardner, J. W., Hines, E. L., Molinier, F., Bartlett, P. N. and Mottram, T. T. [1999] "Prediction of the health of dairy cattle from breath samples using a neural network with parametric model of the dynamic response of an array of semiconducting gas sensors," *Proc. of IEE: Science, Measurement & Technology* **146**(2), 102–106 (JR).

Gardner, J. W., Hines, E. L. and Pang, C. [1996] "Detection of vapours and odours from a multisensor array using pattern recognition: Self-organising adaptive resonance techniques," *Measurement & Control* **29**, 172–178 (JR).

Gardner, J. W. and Iskandarani, M. Z. [1992] "Effect of electrode geometry on gas sensitivity of lead phthalocynine thin film," *Sensors and Actuators B* **9**, 133–142.

Gardner, J. W., Llobet, E. and Hines, E. L. [1999] "PSPICE model for resistive gas and odour sensors," *Proc. IEE Circuits, Devices and Systems* **146**(3), 101–104 (JR).

Gardner, J. W., Shin, H. W., Hines, E. L. and Dow, C. S. [2000] "An electronic nose system for monitoring the quality of potable water," *Sensors and Actuators B* **69**, 336–341 (JR).

Gutierrez-Osuna, R. and Gutierrez-Galvez, A. [2003] "Habituation in the KIII olfactory model with chemical sensor arrays," *IEEE Transactions on Neural Networks* **14**, 1565–1568.

Gutierrez-Osuna, R., Gutierrez-Galvez, A. and Powar, N. U. [2003] "Transient response analysis for temperature modulated chemoresistors,"

*Sensors and Actuators B: Chemical B* **93**(1–3), 57–66.

Gutierrez-Osuna, R. and Nagle, H. T. [1999] "A method for evaluating data-preprocessing techniques for odor classification with an array of gas sensors," *IEEE Transactions on Systems, Man, and Cybernetics B* **29**(5), 626–632.

Gutierrez-Osuna, R. and Powar, N. U. [2003] "Odor mixtures and chemosensory adaptation in gas sensor arrays," *International Journal on Artificial Intelligence Tools* **12**, 1–16.

Hatfield, J. V., Covington, J. A. and Gardner, J. W. [2000] "GasFETs incorporating conducting polymers as gate materials," *Sensors and Actuators B* **65**, 253–256 (JR).

Hines, E. L., Llobet, E. and Gardner, J. W. [1999a] "Neural network based electronic nose for apple ripeness determination," *Electronic Letters* **35**(10), 821–823 (JR).

Hines, E. L., Llobet, E. and Gardner, J. W. [1999b] "Electronic noses: A review of signal processing techniques," *Proc. IEE Circuits, Devices and Systems* **146**(6), 297–310 (JR).

Llobet, E., Hines, E. L., Gardner, J. W. and Franco, S. [1999a] "Non-destructive banana ripeness determination using a neural network based electronic nose," *Measurement Science and Technology* **10**(6), 538–548 (JR).

Llobet, E., Hines, E. L., Gardner, J. W., Bartlett, P. N. and Mottram, T. T. [1999b] "Fuzzy ARTMAP based electronic nose data analysis," *Sensors and Actuators B* **61**, 183–190 (JR).

Marian, S., Tsiulyanu, D., Marian, T. and Liess, H. D. [2001] "Chalcogenide-based chemical sensors foratmospheric pollution control," *Pure Appl. Chem.* **73**(2), 2001–2004.

Mirtaheri, P., Omtveit, T., Klotzbuecher, T., Grimnes, S., Martinsen, Ø. and Tønnessen, T. [2004] "Miniaturization of a biomedical gas sensor," *Physiol. Meas.* **25**, 1511–1522.

Pasini, P., Powar, N., Gutierrez-Osuna, R., Daunert, S. and Roda, A. [2004] "Use of a gas-sensor array for detecting volatile organic compounds in chemically induced cells," *Journal of Analytical and Bioanalytical Chemistry* **378**, 76–83.

Perera, A., Sundic, T., Pardo, A., Gutierrez-Osuna, R. and Marco, S. [2002] "A portable electronic nose based on embedded PC technology and GNU/Linux: Hardware, software and applications," *IEEE Sensors Journal* **2**(3), 235–246.

Shin, H. W., Gardner, J. W. and Hines, E. L. [2000] "An electronic nose system to diagnose illness," *Sensors and Actuators B* **70**, 19–24 (JR).

Vlachos, D. and Avaritsiotis, J. [1996] "Fuzzy neural networks for gas sensing," *Sensors and Actuators B: Chemical* **33**(1–3), 77–82.

Vlachos, D. S., Fragoulis, D. K. and Avaritsiotis, J. N. [1997] "An adaptive neural network topology for degradation compensation of thin film tin oxide gas sensors," *Sensors and Actuators B: Chemical* **45**(3), 223–228.

## Biography

**Mahmoud Z. Iskandarani** received the BEng (Hons.) degree in electronics engineering, the MSc degree in engineering (analogue neural processor) and the PhD in engineering (smart classification and neural networks) from the University of Warwick, UK. He has obtained a Certificate in Non-Destructive Testing from the University of London as well as the Networking Certificate from the Royal Scientific Society in Jordan. His research interests include neural networks, artificial intelligence, smart systems and biometrics.

**Nidal F. Shilbayeh** received the BS degree in computer science from Yarmouk University, Irbid, Jordan in 1988, the MS degree in computer science from Montclair State University, New Jersey, USA in 1992, and the PhD in computer science from Rajesthan University, Rajesthan, India in 1997. He is an associate professor at Jordan University for Graduate Studies. His research interests include embedding, nose system, neural network, image processing, and pattern recognition.